ChemPubSoc Europe

DOI: 10.1002/ejic.201501304

EurJIC European Journal of Inorganic Chemistry

Full Paper

Trackable Therapeutic Agents

Coumarin-Phosphine-Based Smart Probes for Tracking Biologically Relevant Metal Complexes: From Theoretical to Biological Investigations

Lucile Dondaine,[a,b] Daniel Escudero,[c] Moussa Ali,[d] Philippe Richard,[d] Franck Denat,[d] Ali Bettaieb,[a,b] Pierre Le Gendre,[d] Catherine Paul,[a,b] Denis Jacquemin,*[c,e] Christine Goze,*[d] and Ewen Bodio*[d]

Abstract: Ten metal-based complexes and associated ligands have been synthesized and characterized. One of the metal ligands is a coumarin-phosphine derivative, which displays tunable fluorescence properties. The fluorescence is quenched in the case of the free ligand and ruthenium and osmium complexes, whereas it is strong for the gold complexes and phosphonium derivatives. These trends were rationalized by theoretical calculations, which revealed non-radiative channels involving a dark state for the free ligands that is lower in energy than the emissive state and is responsible for the quenching of fluorescence. For the Ru^{II} and Os^{II} complexes, other non-radiative channels involving the manifold of singlet and triplet excited states may play a role. The anti-proliferative properties of all the compounds were evaluated in cancer cell lines (SW480, HCT116, MDA-MB-231 and MCF-7); higher IC_{50} values were obtained for gold(I) complexes, with the free ligands being only weakly cytotoxic.

Introduction

Metal-based complexes are one of the most studied and used classes of anti-cancer drugs. Indeed, cisplatin and platinum derivatives are present in more than 50 % of chemotherapeutic anti-cancer cocktails.[1] Owing to the heavy side-effects of platinum derivatives and to the acquired or intrinsic resistance of some tumours to such treatments, numerous non-platinum metal complexes have been investigated. Among them, ruthenium and gold derivatives have provided the most promising results.[2] Nevertheless, most of these new complexes did not pass clinical trials due to their low efficiency in vivo and the lack of understanding of their mechanism of action [target(s), pharmacokinetics, stability]. This last criterion has become increasingly crucial recently. One possible strategy for tackling this issue is to accumulate data from a large number of biological experiments. More recently, a growing community of chemists have designed trackable therapeutic agents by tethering an imaging probe to the therapeutic moiety. Such objects are sometimes considered as theranostic agents,[3] even though their properties are quite far from Funkhouser's original definition.[4] This new strategy advantageously enables the real-time tracking of drugs in vitro and/or in vivo without altering the cells/animals treated. However, a recurring difficulty is ascertaining whether the whole theranostic agent is actually tracked. Indeed, proving the stability of compounds in complex biological media is not straightforward, and if the integrity of the theranostic is not conserved, it is only the probe moiety that is imaged. One elegant strategy to circumvent this problem is to use smart probes.[5]

Recently, we reported the synthesis, characterization and biological evaluation of several gold(I) coumarin-phosphine complexes, CP-Au-1 and CP-Au-2 (Scheme 1).[5] In this initial study we showed that the coumarin-phosphine ligand presents smart probe character: it displays strong fluorescence when complexed to Au^{I}, but the fluorescence is dramatically quenched in the case of decomplexation (Figure 1). This specific photophysical behaviour enabled us to study its mechanism of action.

In particular, the chlorido-gold analogue CP-Au-1 (Scheme 1) displayed promising results: a valuable cytotoxicity in human

[a] *Ecole Pratique des Hautes Etudes, 75014 Paris, France www.ephe.fr*
[b] *Univ. Bourgogne Franche-Comté, LIIC EA7269, 21000 Dijon, France inserm-u866.u-bourgogne.fr*
[c] *Chimie Et Interdisciplinarité, Synthèse, Analyse, Modélisation (CEISAM), UMR CNRS 6320, BP 92208, Université de Nantes, 2, Rue de la Houssinière, 44322 Nantes Cedex 3, France E-mail: Denis.Jacquemin@univ-nantes.fr www.univ-nantes.fr/jacquemin-d*
[d] *Institut de Chimie Moléculaire de l'Université de Bourgogne Franche-Comté, ICMUB UMR CNRS 6302, 9 avenue Alain Savary, BP 47870, 21078 Dijon Cedex, France E-mail: christine.goze@u-bourgogne.fr ewen.bodio@u-bourgogne.fr www.icmub.fr*
[e] *Institut Universitaire de France (IUF), 1 rue Descartes, 75005 Paris Cedex 05, France www.iufrance.fr*
Supporting information for this article is available on the WWW under http://dx.doi.org/10.1002/ejic.201501304.

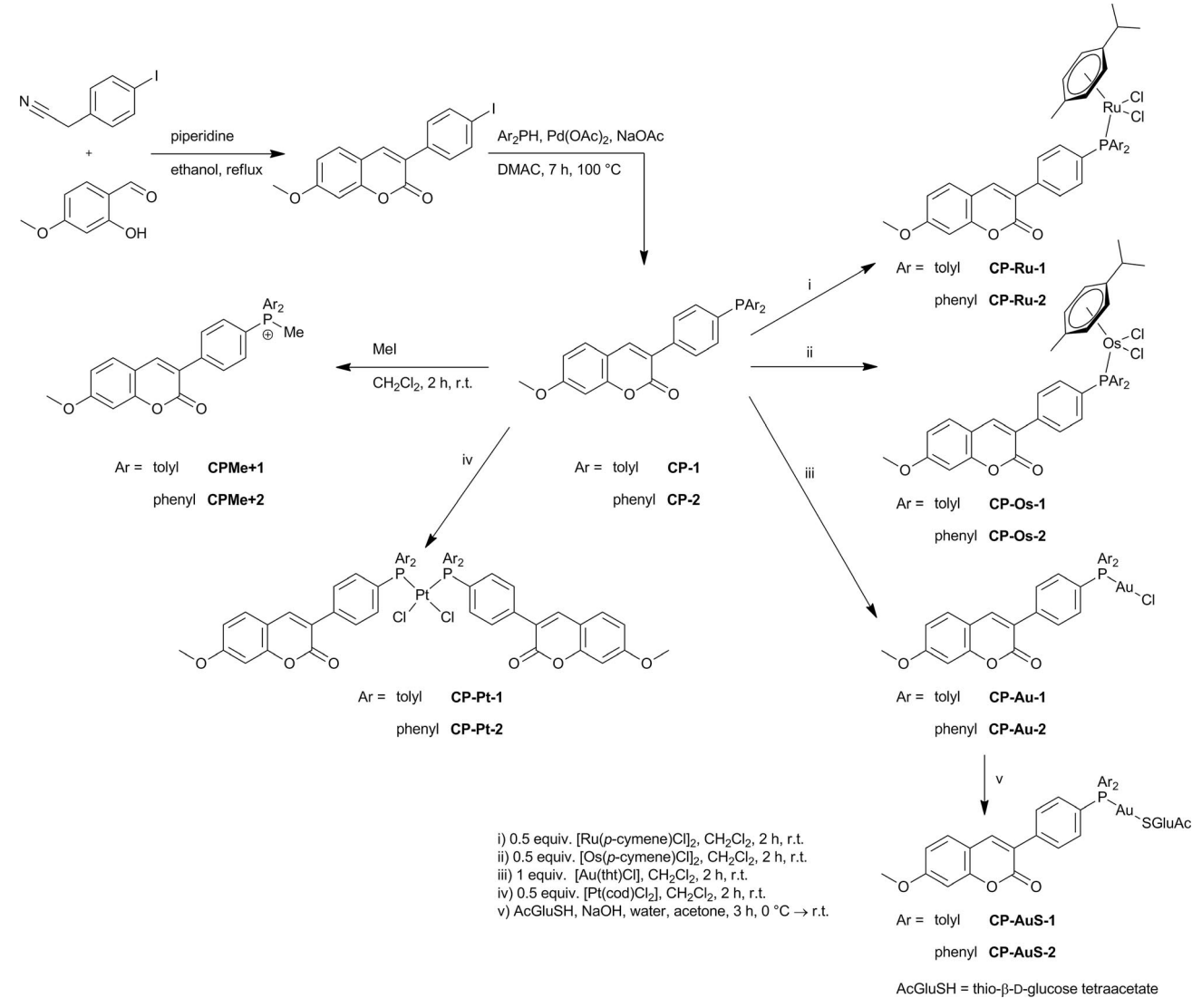

Scheme 1. Synthesis of the phosphoniums CPMe+1 and CPMe+2 and of the complexes CP-Au-1, CP-Au-2, CP-AuS-1, CP-AuS-2, CP-Ru-1, CP-Ru-2, CP-Os-1, CP-Os-2, CP-Pt-1 and CP-Pt-2.

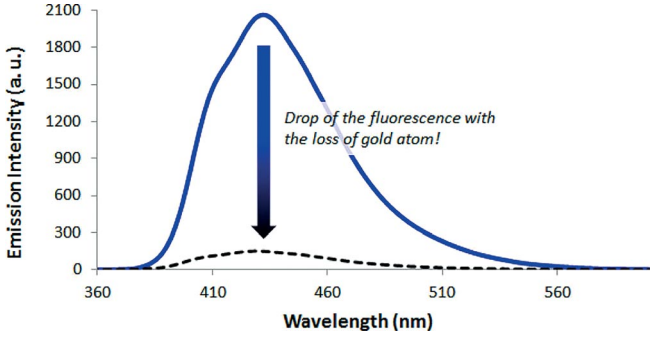

Figure 1. Decrease in fluorescence upon the decomplexation of Au^{I} in CP-Au-1 (reproduced with permission from our previous study[5]).

cancer cells and a low toxicity in healthy zebrafish larvae. In the present study, we wished to generalize this initial investigation by varying the metal centre and, to this end, we selected ruthenium, osmium and platinum, which are all of biological relevance. Our aim was not only to extend the scope of our previous smart theranostics, but to determine whether the coumarin-phosphine ligand could be used as a general tool for tracking transition-metal complexes in vitro.

First, the influence of the metal on the photophysical properties was investigated and particular attention was paid to their ability to quench or otherwise the fluorescence. Theoretical calculations were performed to rationalize these trends. Next, the biological behaviour of the different complexes was evaluated.

Results and Discussion

Chemical Syntheses

The coumarin-phosphine ligands CP-1 and CP-2 were synthesized in two steps according to the procedure described by Pratt and co-workers (Scheme 1).[6] The ligands were then treated either with iodomethane or with metallic precursor

([Au(tht)Cl], [(*p*-cymene)$RuCl_2]_2$, [(*p*-cymene)$OsCl_2]_2$ or [(cod)$PtCl_2$]; tht = tetrahydrothiophene, cod = cycloocta-1,5-diene) to afford the corresponding phosphoniums CPMe+1[5] and CPMe+2, and the metal complexes CP-Au-1,[5] CP-Au-2, CP-Ru-1, CP-Ru-2, CP-Os-1, CP-Os-2, CP-Pt-1 and CP-Pt-2 in excellent yields (Scheme 1).

The complexation reactions were monitored by ^{31}P NMR spectroscopy. The $^{31}P\{^1H\}$ NMR spectra of the ligands display a singlet at around –7 ppm, whereas the gold complexes display a singlet at around 32 ppm, the ruthenium complexes a singlet at around 22 ppm and the osmium complexes a singlet at around –14 ppm (this negative chemical shift could be regarded as surprising but it is in fact expected for osmium–phosphine complexes).[7] The platinum derivatives gave a slightly more complex signal: the complexes display a single resonance in the $^{31}P\{^1H\}$ NMR spectra with platinum satellites separated by a coupling constant $^1J(^{195}Pt–P)$ of 3675 Hz, which indicates the presence of the chlorine atoms *trans* to the phosphorus atoms and thus a *cis* geometry.[8] Two additional gold(I) complexes were synthesized by treating the chlorido–gold complexes CP-Au-1 and CP-Au-2 with the in situ generated thiolate of thioglucose tetraacetate. CP-AuS-1[5] and CP-AuS-2 were obtained in high yields (Scheme 1).

All the compounds were fully characterized and the structures of compounds CP-1,[5] CP-2, CP-Au-1[5] and CP-Ru-2 were confirmed by single-crystal X-ray diffraction analysis (Figure 2).[9] CP-2 crystallizes in the $P\bar{1}$ space group and CP-Ru-2 crystallizes in the monoclinic $P2_1/n$ space group. The asymmetric unit contains two independent molecules and one CH_2Cl_2 solvate molecule. The two independent molecules of the CP-Ru-2 cell share the same conformation (RMSD = 0.116 Å after inversion of one molecule). The Ru group adopts the classical piano stool geometry.

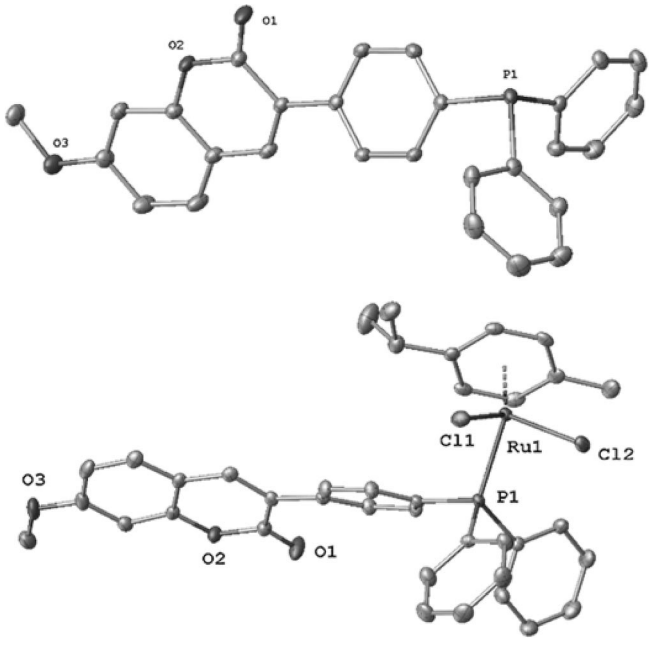

Figure 2. ORTEP views of CP-2 (top) and CP-Ru-2 (bottom). The CH_2Cl_2 molecule is not shown for clarity and only one of the two independent molecules is represented (see our previous study[5] for the ORTEP views of CP-1 and CP-Au-1).

Photophysical Studies

The photophysical characterization of the ligands CP-1 (tolyl) and CP-2 (phenyl) and the different complexes was carried out in dichloromethane and the data are summarized in Table 1.

Table 1. Photophysical data[a] for the different compounds in CH_2Cl_2 at 298 K.

	λ_{abs} [nm]	λ_{em} [nm]	ε [M^{-1} cm^{-1}]	Φ_f [b] [%]	Br [M^{-1} cm^{-1}]	Br/Br(L)
CP-1	348	430	25100	3.1	778	1
CPMe+1	355	441	34300	91	31213	40[c]
CP-Au-1	350	432	25700	83	21331	27
CP-AuS-1	349	432	26200	83	21746	28
CP-Ru-1	348	433	26600	5.8	1543	2
CP-Os-1	346	432	21800	9.5	2071	3
CP-Pt-1	346	432	59900	4.8	2875	4
CP-2	348	430	25000	5	1250	1
CPMe+2	360	440	23100	98	22638	18[c]
CP-Au-2	348	430	28600	92	26312	21
CP-AuS-2	350	433	24300	95	23085	18
CP-Ru-2	352	428	31000	7.5	2325	2
CP-Os-2	350	430	28800	1.3	374	0.3
CP-Pt-2	350	433	58300	4	2332	2

[a] λ_{abs} = wavelength of maximal absorption; λ_{em} = wavelength of maximal emission; ε = molar absorption coefficient; Φ_f = fluorescence quantum yield; brightness, Br = $\varepsilon\Phi_f$; Br(L) = brightness of ligand CP-1 or CP-2. [b] Reference: diphenylanthracene (Φ_f = 0.97, λ_{exc} = 355 nm, in cyclohexane).[10] [c] This ratio, which illustrates the smart-probe character of the compounds, is not relevant for the phosphonium derivatives because the "demethylation" of CPMe+1 and CPMe+2 is very unlikely.

UV/Visible Studies

The ligands CP-1 and CP-2 each present an absorption maximum at 348 nm in CH_2Cl_2, which corresponds to the S_1 band (see Theoretical Calculations section below), and have molar absorption coefficients of 25100 and 25000 M^{-1} cm^{-1}, respectively, which are characteristic of the coumarin signature.[6] A small shoulder can be additionally observed for all the compounds at the beginning of the S_1 band (at around 300–320 nm), which may correspond to the S_2 transition or to a vibronic coupling effect. These bands have readily been assigned to spin-allowed π–π* transitions. Alkylation of the phosphine induces a bathochromic shift of the absorption band of about 10 nm. Complexation to Au^I, Ru^{II} or Os^{II} did not significantly influence the molar absorption coefficients. A low-intensity broad shoulder can be seen at 490 and 450 nm for the Ru^{II} and Os^{II} complexes, respectively, which correspond to metal-centred bands (see below). Finally, the presence of two coumarin chromophores in the Pt^{II} complexes CP-Pt-1 and CP-Pt-2 increases their absorption coefficients to 59900 and 58300 M^{-1} cm^{-1}, respectively. These values are twice those obtained for structures bearing a single coumarin fluorophore.

Exemplarily, the absorption and emission spectra of CP-2 and CP-Ru-2 are represented in Figure 3 (see the Supporting Information for the spectra of the other compounds).

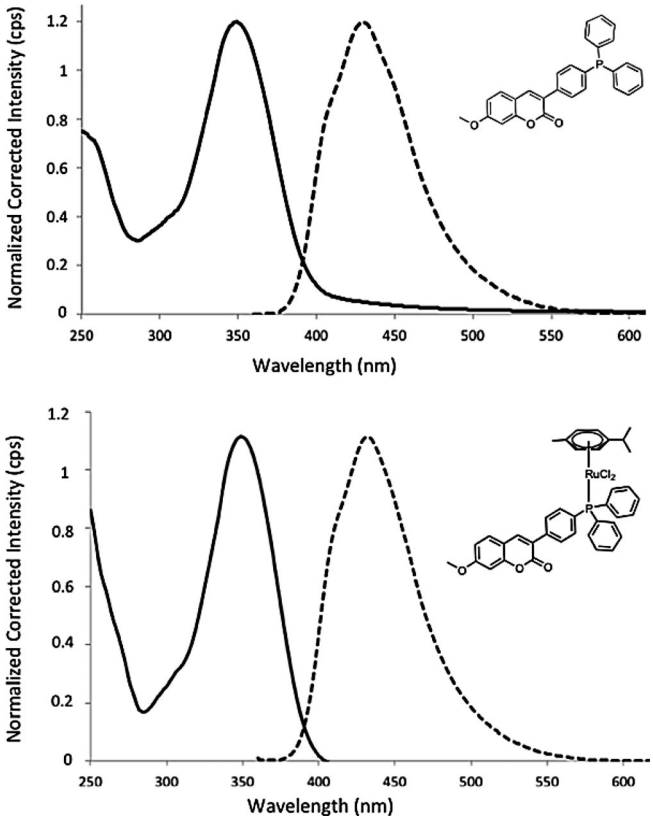

Figure 3. Absorption (solid line) and emission (dashed line) spectra of CP-2 (top) and CP-Ru-2 (bottom) in CH_2Cl_2 at 298 K.

Emission Properties

For all systems, a fluorescence band peaking at around 430 nm can be observed, which corresponds to the emission of the coumarin moiety. However, the rate of fluorescence significantly depends upon the compound. First, the quantum yields of the ligands CP-1 and CP-2 are relatively low (3.1 and 5 %, respectively). This quenching is primarily attributed in the photophysics community to a photoinduced electron transfer (PET) from the phosphine to the fluorophore. As a result of our theoretical studies (see below), we herein propose that non-radiative channels involving a dark state are responsible for the observed quenching of photoluminescence. The dark state is precisely the charge transfer that results from PET, and hence it further validates our hypothesis. Alkylation of the phosphine results in a strong enhancement of the fluorescence of the coumarin (Φ = 91 % for CPMe+1 and 98 % for CPMe+2), because the non-radiative channels are efficiently suppressed. Complexation with Au^{I}, which is an inert d^{10} metal, induces the same phenomenon as alkylation of the phosphine, that is, blockage of the lone pair on the phosphine. The resulting quantum yields of the different Au complexes are therefore very high (between 83 and 95 %).

On the other hand, complexation with Ru^{II}, Os^{II} and Pt^{II} strongly quenches the fluorescence of the coumarin. Even if the quenching mechanism is also prevented in these compounds, additional photophysical phenomena, which induce a decrease in the fluorescence quantum yields, are involved. These mechanisms could involve electron-transfer phenomena or triplet excited-state deactivation pathways that can be reached by intersystem-crossing mechanisms. Indeed, the presence of metal ions can induce the population of metal-to-ligand charge-transfer (^{3}MLCT) states and the eventual appearance of non-radiative deactivation pathways involving metal-centred (^{3}MC) states.

The brightness values are moderate to high. Therefore, all the complexes, except CP-Os-2 and maybe CP-Ru-1, could most probably be tracked in vitro in the micromolar range. The "smart-probe character" of the complexes can be evaluated by the ratio of the brightness of the complexes to the brightness of the corresponding coumarin-phosphine ligand CP-1 or CP-2 (Table 1). As a result of the decrease in the quantum yields for the Ru^{II}, Os^{II} and Pt^{II} complexes, this ratio is poor (0.3 to 4). Thus, the decrease in fluorescence upon decomplexation would not be sufficient to obtain an unambiguous in vitro interpretation. In contrast, all gold complexes display very good ratios, from 18 to 28, thereby confirming previous observations.[5]

Theoretical Calculations

To gain insights into the photophysical properties of the coumarin-phosphine ligands and their complexes, we performed DFT and time-dependent DFT (TD-DFT) calculations (see Computational Details in the Exp. Sect.). Table 2 lists the TD-B3LYP vertical excitation energies and oscillator strengths for the main lowest singlet excited states of CP-1, CPMe+1, CP-Au-1 and CP-Ru-1.

Two singlet excited states of mixed $n_P/\pi_{coum}\rightarrow\pi^*_{coum}$ character (see the specific excitations in Table 2 and the orbitals involved in Figure 4, c) contribute to the main UV/Vis band of CP-1, which shows a peak experimentally at 350 nm. These excited

Table 2. TD-B3LYP/6-31G(d) vertical singlet electronic transition energies (in nm and eV) and oscillator strengths of CP-1, CPMe+1, CP-Au-1 and CP-Ru-1. The main molecular orbital contributions are given in each case.

	State	λ [nm/eV][a]	f [a.u.][a]	Character [Coeff.][a]
CP-1	S_1	375/3.31	0.447	(H→L) $n_P\pi_{coum}\rightarrow\pi^*_{coum}$ [0.70]
		370/3.35	*0.705*	(*H→L*) $n_P\pi_{coum}\rightarrow\pi^*_{coum}$ [*0.70*]
	S_2	326/3.80	0.442	(H-1→L) $\pi_{coum}n_P\rightarrow\pi^*_{coum}$ [0.69]
		327/3.79	*0.311*	(*H-1→L*) $\pi_{coum}n_P\rightarrow\pi^*_{coum}$ [*0.69*]
CPMe+1	S_1	385/3.21	0.827	(H→L) $\pi_{coum}\rightarrow\pi^*_{coum}$ [0.70]
CP-Au-1	S_1	348/3.57	0.941	(H→L) $\pi_{coum}\rightarrow\pi^*_{coum}$ [0.70]
CP-Ru-1	S_1	550/2.25	0.007	(H→L + 1) $4d_{t2g}\rightarrow4d_{eg}\pi^*_{arene}$ [0.63]
	S_4	455/2.73	0.015	(H-1→L + 1) $4d_{t2g}\rightarrow4d_{eg}\pi^*_{arene}$ [0.42]
	S_{10}	350/3.55	0.843	(H-3→L) $\pi_{coum}\rightarrow\pi^*_{coum}$ [0.70]

[a] PCM-TD-B3LYP/6-31G(d) values in CH_2Cl_2 are given in italics.

states are theoretically located at 375 and 326 nm, and they gain intensity mainly from their $\pi_{coum}\rightarrow\pi^*_{coum}$ contribution. The inclusion of solvent effects leads to very small shifts of these excited states (ca. 0.01–0.04 eV, see Table 2). In the case of the methylated CPMe+1 ligand and the CP-Au-1 complex, only the S_1 state contributes to the experimental peaks observed at 355 and 350 nm, respectively; good agreement with the TD-B3LYP values (385 and 348 nm, respectively) is reached. For CP-Ru-1, the first nine singlets involve the $RuCl_2$–arene core, see exemplarily the S_1 and S_4 states in Table 2. These states possess very low oscillator strengths and they accordingly contribute to the small broad tail extending up to 550 nm in the recorded spectrum (see Figure 3). The $\pi_{coum}\rightarrow\pi^*_{coum}$ excitation (S_{10}) is responsible for the main UV/Vis band of CP-Ru-1, and its position is again in very good agreement with the experimental value.

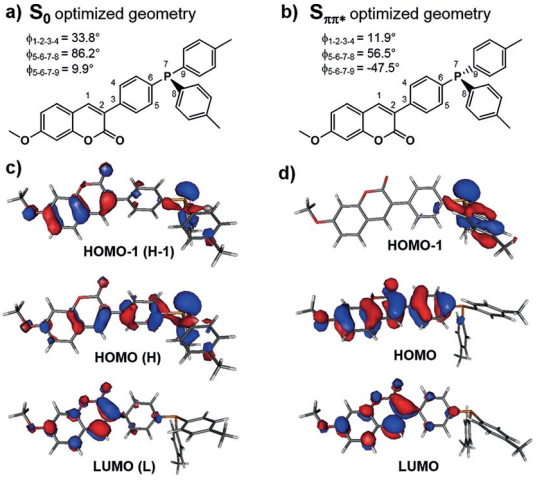

Figure 4. Main geometrical features of the S_0 (a) and $S_{\pi\pi^*}$ (b) optimized geometries of CP-1. Kohn–Sham (KS) orbitals involved in the lowest excitations of CP-1 in its S_0 (c) and $S_{\pi\pi^*}$ (d) optimized geometries.

We next evaluated the emission properties and the quenching of fluorescence in CP-1. Table 3 lists the TD-B3LYP emission energies for the optimized structures of the emissive state ($S_{\pi\pi^*}$) of CP-1 and CPMe+1. The TD-B3LYP emission energies are in reasonable agreement with experimental evidence. The main geometrical features of the S_0 and $S_{\pi\pi^*}$ optimized geometries of CP-1 are highlighted in Figure 4, a,b. Relaxation of its $S_{\pi\pi^*}$ potential energy surface (PES) leads to 1) a coplanarization of coumarin and its adjacent tolyl ligand (see the $\phi_{1-2-3-4}$ dihedral angle in Figure 4, b) and 2) a twist of the $Ptol_2$ moiety (compare the $\phi_{5-6-7-8}$ and $\phi_{5-6-7-9}$ dihedral angles in Figure 4, a,b). In the optimized S_0 geometry, both the HOMO–1 and HOMO orbitals are delocalized over the phosphine and coumarin moieties (see Figure 4, c). In contrast, in the optimized $S_{\pi\pi^*}$ geometry, these orbitals evolve to well-separated n_P and π_{coum} orbitals (see HOMO–1 and HOMO in Figure 4, d). Consequently, pure $n_P\pi^*_{coum}$ and $\pi_{coum}\pi^*_{coum}$ excited states are obtained for the latter geometry (see Table 3). For this geometry, the dark $n_P\pi^*_{coum}$ state is located 0.16 eV below the emissive $\pi_{coum}\pi^*_{coum}$ state. In this simplified photophysical picture for CP-1, both the S_1 and S_2 states will be populated in the Franck–Condon region. From there, internal conversion processes will predominantly lead to the population of the lowest-lying $n_P\pi^*_{coum}$ state. A very small fluorescence rate (k_{fl}) is expected from this state (see its negligible oscillator strength in Table 3). Therefore, instead of radiative emission from the $S_{\pi\pi^*}$ state, competing non-radiative decay channels leading to S_0 will be favoured for CP-1. These are presumably the ultimate reasons for the observed quenching of fluorescence in CP-1. We remark that this theoretical modelling provides support for a non-radiative interpretation of the quenching of fluorescence rather than an intramolecular photoinduced electron transfer (PET) mechanism. To the best of our knowledge, only one previous theoretical study proposed a similar non-radiative decay path for rhodamines.[11] In contrast, these non-radiative decay channels are not available for CPMe+1 or CP-Au-1 (their lowest excited state is the bright $S_{\pi\pi^*}$ state, see Table 3 exemplarily for CPMe+1). Finally, other non-radiative mechanisms involving the manifold of $RuCl_2$-based singlet and triplet states are opened up for CP-Ru-1. These states are known to be involved in non-radiative deactivation pathways involving crossings with the ground-state PES.[12] These non-radiative channels might compete with PET.[13]

Table 3. TD-B3LYP/6-31G(d) vertical singlet electronic emission energies (in nm and eV) and oscillator strengths of CP-1 and CP-Au-1 for their $S_{\pi\pi^*}$ optimized geometries. The main molecular orbital contributions are given in each case.

	State	λ [nm/eV]	f [a.u.]	Character [coeff.]
CP-1	S_1	428/2.90	0.000	$n_P\rightarrow\pi^*_{coum}$ [0.70]
	S_2	405/3.06	0.911	$\pi_{coum}\rightarrow\pi^*_{coum}$ [0.70]
CPMe+1	S_1	414/3.00	0.825	$\pi_{coum}\rightarrow\pi^*_{coum}$ [0.70]

Biological Studies

The anti-proliferative activity of the coumarin-derivatives was tested on four human cancer cell lines of mammary (MDA-MB-231 and MCF-7) or colon (SW480 and HCT116) origins (Table 4).

Table 4. IC_{50} values for the different coumarin derivatives against SW480, HCT116, MDA-MB-231 and MCF-7 cells determined in MTS assays for 48 h.

	IC_{50} [μM]			
	SW480	HCT116	MDA-MB-231	MCF-7
CP-1	160 ± 13	122 ± 5	>200	135 ± 14
CPMe+1[a]	25.7 ± 0.3	10.1 ± 0.2	33 ± 14	28 ± 4
CP-Au-1[a]	42 ± 11	38 ± 17	33 ± 15	49 ± 1
CP-AuS-1[a]	34 ± 14	49.9 ± 0.3	46 ± 5	50.1 ± 0.1
CP-Ru-1	75 ± 25	74.9 ± 0.1	74.9 ± 0.1	83 ± 15
CP-Os-1	42 ± 14	53 ± 14	50.0 ± 0,1	50.0 ± 0.3
CP-Pt-1	insoluble			
CP-2	>200	104 ± 28	74.8 ± 0.2	>200
CPMe+2	75.6 ± 0.7	75.9 ± 0.8	47 ± 5	75.3 ± 0.5
CP-Au-2	25.1 ± 0.1	26 ± 1	25.3 ± 0.4	25.3 ± 0.2
CP-AuS-2	25.2 ± 0.1	25.5 ± 0.1	24.5 ± 0.3	24.8 ± 0.1
CP-Ru-2	73 ± 7	49.4 ± 0.5	25.3 ± 0.2	49.8 ± 0.3
CP-Os-2	105 ± 27	86 ± 13	50 ± 1	74.7 ± 0.1
CP-Pt-2	49	64 ± 26	58 ± 11	>200

[a] Determined previously, see ref.[5]

An overview of the data indicated that the CP-1 and CP-2 ligands are weakly cytotoxic and that the different metal-based coumarin complexes are more potent towards the MDA-MB-231

cell line than towards the SW480, HCT116 and MCF-7 cell lines. The complexes show substantial toxic effects with IC_{50} values ranging from 24 to 106 μM. Among the metal complexes, the gold(I) derivatives display the more promising properties (with IC_{50} ranging from 24.5 to 50.1 μM) and the general trend suggests that the phenyl derivatives are a little more potent than the tolyl derivatives. In contrast, the Os^{II} complexes present higher IC_{50} values, which may be due to their lower solubility. Additionally, we note that the "X-type"[14] ligand present in the gold complex (chlorido or thioglucose tetraacetate ligand) does not seem to influence the in vitro cytotoxic properties of the gold complexes (CP-Au-1 and CP-AuS-1 vs. CP-Au-2 and CP-AuS-2). However, even if there is no notable difference in vitro, the pharmacokinetic properties and the biodistribution of the complexes will probably be different in vivo. Surprisingly, the phosphonium derivative CPMe+2 is significantly less cytotoxic than its tolyl analogue CPMe+1 (up to 7.5 times in HCT116). Concerning the Pt complexes CP-Pt-1 and CP-Pt-2, the IC_{50} values are not really relevant, when determined, due to their poor water solubility. CP-Pt-1 was even almost insoluble in pure DMSO.

Conclusions

We have designed, synthesized and characterized eight new metal-based theranostic agents. The photophysical properties were studied and compared. As highlighted in some of our previous work on BODIPY derivatives, gold derivatives gave the most promising results and only the gold(I)–coumarin complexes could be considered as smart theranostic compounds.[5,7,15] The quenching of the fluorescence of the ligands and Ru^{II} complexes has been explained by theoretical calculations. Indeed, non-radiative channels involving a dark state, which is lower in energy than the emissive state, are responsible for the quenching of fluorescence. In the Ru^{II} and Os^{II} complexes, other non-radiative channels involving the manifold of singlet and triplet excited states might be operative and explain the quenching. The anti-proliferative properties of all the compounds were evaluated on SW480, HCT116, MDA-MB-231 and MCF-7 cell lines. The ligands appeared to be weakly cytotoxic, whereas the complexes produced interesting IC_{50} values, especially for the MDA cell line (with the exception of the poorly soluble Pt^{II} complex CP-Pt-1). The most interesting IC_{50} values were obtained for the gold(I) complexes as well as the phosphonium derivatives. It is worth noting that even if the smart-probe character is a bit less pronounced for the diphenylphosphine derivatives compared with the ditolylphosphines, their anti-proliferative properties are improved.

As a consequence of the results described here, we are now focusing our attention on gold(I) complexes by varying the substituent groups on the phosphorus atom combined with water-solubilizing groups.

Experimental Section

General: All the reactions were carried out under purified argon using Schlenk techniques. Solvents were dried and distilled under argon before use. All other reagents were commercially available and used as received. CP-1, CPMe+1, CP-Au-1, CP-AuS-1 and CP-2 were synthesized according to literature procedures.[5,6] All the analyses were performed at the Plateforme d'Analyses Chimiques et de Synthèse Moléculaire de l'Université de Bourgogne. The identities and purities (≥95 %) of the complexes were unambiguously established by HRMS and NMR spectroscopy. The exact masses of the synthesized complexes were determined with a Thermo LTQ Orbitrap XL spectrometer. ^{1}H (300.13 MHz), ^{13}C (75.47 MHz) and ^{31}P (121.49 MHz) NMR spectra were recorded with a Bruker 300 Avance III spectrometer. Chemical shifts (δ) are quoted in ppm relative to TMS (^{1}H and ^{13}C) using the residual protonated solvent (^{1}H) or the deuterated solvent (^{13}C) as internal standards; 85 % H_3PO_4 (^{31}P) was used as an external standard. The atom labelling used for the NMR assignments is presented in Figure 5. IR spectra were recorded with a Bruker Vector 22 FT-IR spectrophotometer (Golden Gate ATR).

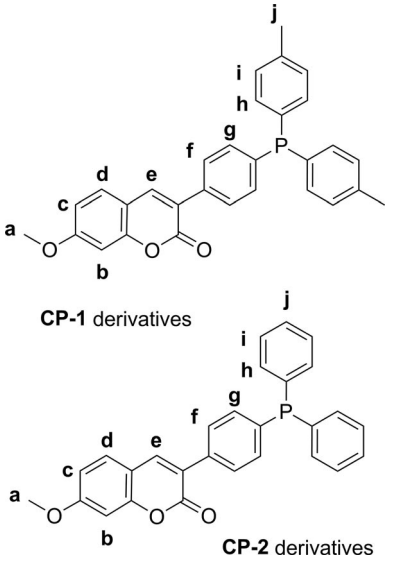

Figure 5. Arbitrary labelling of the ligand protons.

[(η⁶-*p*-Cymene)(3-{4-(di-*p*-tolylphosphanyl)phenyl}-7-methoxy-2*H*-chromen-2-one)$RuCl_2$] (CP-Ru-1): The reaction was carried out under argon. 3-[4-(Di-*p*-tolylphosphino)phenyl]-7-methoxy-2*H*-chromen-2-one (CP-1; 150 mg, 0.323 mmol) and $[RuCl_2(p\text{-cymene})]_2$ (99 mg, 0.162 mmol) were dissolved in degassed CH_2Cl_2 (10 mL). The resulting mixture was stirred at room temperature for 2 h. The reaction was monitored by ^{31}P NMR spectroscopy. Upon completion, the solvent was removed under reduced pressure. The ruthenium complex CP-Ru-1 was isolated as a red powder (208 mg, 84 % yield). ^{1}H NMR ($CDCl_3$): δ = 1.11 [d, $^{3}J_{H,H}$ = 6.9 Hz, 6 H, $CH(CH_3)_2$ *p*-cymene], 1.88 (s, 3 H, CH_3 *p*-cymene), 2.36 (6 H, H_j), 2.87 [hept, $^{3}J_{H,H}$ = 6.9 Hz, 1 H, $CH(CH_3)_2$ *p*-cymene], 3.88 (s, 3 H, H_a), 4.99 (dd, $^{3}J_{H,H}$ = 6.2, $^{4}J_{H,P}$ = 1.0 Hz, 2 H, CH_{Ar} *p*-cymene), 5.21 (d, $^{3}J_{H,H}$ = 6.2 Hz, 2 H, CH_{Ar} *p*-cymene), 6.83–6.89 (m, 2 H, $H_{b,c}$), 7.18 (dd, $^{3}J_{H,H}$ = 8.2, $^{4}J_{H,P}$ = 1.8 Hz, 4 H, H_i), 7.43 (d, $^{3}J_{H,H}$ = 8.4 Hz, 1 H, H_d), 7.65 (dd, $^{3}J_{H,H}$ = 8.5, $^{4}J_{H,P}$ = 2.0 Hz, 2 H, H_f), 7.69–7.78 (m, 5 H, $H_{e,h}$), 7.83–7.90 (m, 2 H, H_g) ppm. $^{13}C\{^{1}H\}$ NMR ($CDCl_3$): δ = 18.0, 21.5, 22.0, 30.4, 56.0, 87.4 (d, $J_{C,P}$ = 5.5 Hz), 89.0 (d, $J_{C,P}$ = 3.1 Hz), 96.0, 100.6, 111.2 (d, $J_{C,P}$ = 3.1 Hz), 113.0, 113.4, 123.9 (d, $J_{C,P}$ = 1.1 Hz), 127.7 (d, $J_{C,P}$ = 9.9 Hz), 128.9 (d, $J_{C,P}$ = 10.3 Hz), 129.3, 130.6 (d, $J_{C,P}$ = 47.2 Hz), 134.4 (d, $J_{C,P}$ = 46.2 Hz), 134.5 (d, $J_{C,P}$ = 9.9 Hz), 134.5 (d, $J_{C,P}$ = 9.4 Hz), 136.6 (d, $J_{C,P}$ = 2.8 Hz), 140.6 (d, $J_{C,P}$ = 2.8 Hz), 140.9, 155.6, 160.8, 163.1 ppm. $^{31}P\{^{1}H\}$ NMR ($CDCl_3$): δ = 23.2 ppm. UV/Vis (CH_2Cl_2): λ_{max} (ε) = 348 nm (26600 M^{-1} cm^{-1}). IR: $\tilde{\nu}$ = 1653

($\nu_{C=O}$) cm^{-1}.HRMS (ESI): calcd. for $C_{40}H_{39}ClO_3PRu$ 735.13712 [M – Cl]$^+$; found 735.13984.

[(η^6-*p*-Cymene)(3-{4-(di-*p*-tolylphosphanyl)phenyl}-7-methoxy-2*H*-chromen-2-one)OsCl$_2$] (CP-Os-1): The reaction was carried out under argon. CP-1 (132 mg, 0.285 mmol) and [$OsCl_2$(*p*-cymene)]$_2$ (113 mg, 0.142 mmol) were dissolved in degassed CH_2Cl_2 (10 mL). The resulting mixture was stirred at room temperature for 2 h. The reaction was monitored by ^{31}P NMR spectroscopy (242.9 MHz, 300 K). Upon completion, the solvent was removed under reduced pressure. The osmium complex CP-Os-1 was isolated as pale-brown powder (193 mg, 79 % yield). ^{1}H NMR ($CDCl_3$): δ = 1.16 [d, $^3J_{H,H}$ = 6.9 Hz, 6 H, CH(C*H*$_3$)$_2$ *p*-cymene], 1.98 (s, 3 H, C*H*$_3$ *p*-cymene), 2.36 (6 H, H$_j$), 2.76 [hept, $^3J_{H,H}$ = 6.9 Hz, 1 H, C*H*(CH$_3$)$_2$ *p*-cymene], 3.88 (s, 3 H, H$_a$), 5.18 (d, $^3J_{H,H}$ = 5.7 Hz, 2 H, C*H*$_{Ar}$ *p*-cymene), 5.42 (d, $^3J_{H,H}$ = 5.7 Hz, 2 H, C*H*$_{Ar}$ *p*-cymene), 6.83–6.88 (m, 2 H, H$_{b,c}$), 7.18 (dd, $^3J_{H,H}$ = 8.2, $^4J_{H,P}$ = 1.8 Hz, 4 H, H$_i$), 7.43 (d, $^3J_{H,H}$ = 8.4 Hz, 1 H, H$_d$), 7.62–7.70 (m, 6 H, H$_{f,h}$), 7.77–7.85 (m, 3 H, H$_{e,g}$) ppm. ^{13}C{^{1}H} NMR ($CDCl_3$): δ = 18.0, 21.5, 22.4, 30.2, 56.0, 80.1 (d, $J_{C,P}$ = 5.1 Hz), 80.3 (d, $J_{C,P}$ = 2.5 Hz), 88.6, 100.6, 103.5 (d, $J_{C,P}$ = 4.0 Hz), 113.0, 113.4, 123.9, 127.6 (d, $J_{C,P}$ = 10.4 Hz), 128.8 (d, $J_{C,P}$ = 10.4 Hz), 129.3, 130.1 (d, $J_{C,P}$ = 54.4 Hz), 134.0 (d, $J_{C,P}$ = 52.6 Hz), 134.6 (d, $J_{C,P}$ = 9.8 Hz), 134.7 (d, $J_{C,P}$ = 9.8 Hz), 136.6 (d, $J_{C,P}$ = 2.7 Hz), 140.7 (d, $J_{C,P}$ = 2.1 Hz), 140.9, 155.6, 160.8, 163.0 ppm. ^{31}P{^{1}H} NMR ($CDCl_3$): δ = –14.1 ppm. UV/Vis (CH_2Cl_2): λ_{max} (ε) = 346 nm (26600 M^{-1} cm^{-1}). IR: $\tilde{\nu}$ = 1653 ($\nu_{C=O}$) cm^{-1}. HRMS (ESI): calcd. for $C_{40}H_{39}ClO_3POs$ 825.194 [M – Cl]$^+$; found 825.19609.

[Bis(3-{4-(di-*p*-tolylmethylphosphanyl)phenyl}-7-methoxy-2*H*-chromen-2-one)PtCl$_2$] (CP-Pt-1): The reaction was carried out under argon. 3-[4-(Di-*p*-tolylphosphino)phenyl]-7-methoxy-2*H*-chromen-2-one (CP-1; 150 mg, 0.323 mmol) and cyclooctadieneplatinum(II) dichloride (60.4 mg, 0.161 mmol) were dissolved in degassed CH_2Cl_2 (10 mL). The resulting mixture was stirred at room temperature for 2 h. The reaction was monitored by ^{31}P NMR spectroscopy (242.9 MHz, 300 K). Upon completion, the solvent was removed under reduced pressure. The platinum complex CP-Pt-1 was isolated as a yellow powder (360 mg, 92 % yield). ^{1}H NMR ($CDCl_3$): δ = 2.34 (12 H, H$_j$), 3.89 (s, 6 H, H$_a$), 6.82–6.90 (m, 4 H, H$_{b,c}$), 6.99 (br. d, $^3J_{H,H}$ = 7.1 Hz, 8 H, H$_i$), 7.34–7.58 (m, 18 H, H$_{d,f,g,h}$), 7.81 (br. s, 2 H, H$_e$) ppm. ^{13}C{^{1}H} NMR ($CDCl_3$): δ = 21.4, 55.8, 100.4, 113.1 (d, $J_{C,P}$ = 20.5 Hz), 123.1, 126.4, 127.4, 128.6, 128.7, 128.8, 129.4, 134.2, 135.0, 135.1, 141.2, 141.3, 155.5, 160.6, 163.0 ppm. ^{31}P{^{1}H} NMR ($CDCl_3$): δ= 12.6 (s+d, $^1J_{P,Pt}$ = 3675 Hz) ppm. UV/Vis (CH_2Cl_2): λ_{max} (ε) = 346 nm (59900 M^{-1} cm^{-1}). IR: $\tilde{\nu}$ = 1653 ($\nu_{C=O}$) cm^{-1}. HRMS (ESI): calcd. for $C_{60}H_{50}ClO_3P_2Pt$ 1158.24183 [M – Cl]$^+$; found 1158.24245.

3-[4-(Methyldiphenylphosphonium)phenyl]-7-methoxy-2*H*-chromen-2-one Iodide (CPMe+2) : The reaction was carried out under argon. CP-1 (100 mg, 0.229 mmol) and iodomethane (49 mg, 0.343 mmol) were dissolved in degassed CH_2Cl_2 (7 mL). The resulting mixture was stirred at room temperature for 2 h. The reaction was monitored by ^{31}P NMR spectroscopy. Upon completion, the solvent was removed under reduced pressure. The phosphonium CPMe+2 was isolated as a yellow powder (127 mg, 96 % yield). ^{1}H NMR ($CDCl_3$): δ = 3.16 (d, $^2J_{H,P}$ = 13.4 Hz, 3 H, P-C*H*$_3$), 3.89 (s, 3 H, H$_a$), 6.82 (d, $^4J_{H,H}$ = 2.4 Hz, 1 H, H$_b$), 6.88 (dd, $^3J_{H,H}$ = 8.6, $^4J_{H,H}$ = 2.4 Hz, 1 H, H$_c$), 7.61–7.86 (m, 13 H, H$_{d,g,h,i,j}$), 8.11 (dd, $^3J_{H,H}$ = 8.7, $^4J_{H,P}$ = 3.1 Hz, 2 H, H$_f$), 8.20 (s, 1 H, H$_e$) ppm. ^{13}C{^{1}H} NMR ($CDCl_3$): δ = 11.6 (d, $J_{C,P}$ = 57.3 Hz), 56.1, 100.6, 113.2 (d, $J_{C,P}$ = 14.0 Hz), 117.8 (d, $J_{C,P}$ = 89.9 Hz), 118.5, 119.7, 121.5 (d, $J_{C,P}$ = 1.2 Hz), 130.3, 130.3 (d, $J_{C,P}$ = 13.2 Hz),130.6, 130.8, 133.4 (d, $J_{C,P}$ = 10.9 Hz), 133.6 (d, $J_{C,P}$ = 11.4 Hz), 135.4 (d, $J_{C,P}$ = 2.8 Hz), 142.2 (d, $J_{C,P}$ = 3.0 Hz), 143.1, 155.9, 160.5, 163.8 ppm. ^{31}P{^{1}H} NMR ($CDCl_3$): δ = 21.2 ppm. UV/Vis (CH_2Cl_2): λ_{max} (ε) = 360 (23100 M^{-1} cm^{-1}). IR: $\tilde{\nu}$ = 1653 ($\nu_{C=O}$) cm^{-1}. HRMS (ESI): calcd. for $C_{29}H_{24}O_3P^+$ 451.14576 [M – I]$^+$; found 451.14421.

[(3-{4-(Diphenylphosphanyl)phenyl}-7-methoxy-2*H*-chromen-2-one)AuCl] (CP-Au-2): The reaction was carried out under argon. 3-[4-(Diphenylphosphino)phenyl]-7-methoxy-2*H*-chromen-2-one (CP-2; 200 mg, 0.46 mmol) and [Au(tht)Cl] (147 mg, 0.46 mmol) were dissolved in degassed CH_2Cl_2 (12 mL). The resulting mixture was stirred at room temperature for 2 h. The reaction was monitored by ^{31}P NMR spectroscopy. Upon completion, the solvent was removed under reduced pressure. The gold complex CP-Au-1 was isolated as a yellow powder (285 mg, 93 % yield). ^{1}H NMR ($CDCl_3$): δ = 3.90 (s, 3 H, H$_a$), 6.87 (d, $^4J_{H,H}$ = 2.4 Hz, 1 H, H$_b$), 6.90 (dd, $^3J_{H,H}$ = 8.4, $^4J_{H,H}$ = 2.4 Hz, 1 H, H$_c$), 7.43–7.63 (m, 13 H, H$_{d,g,h,i,j}$), 7.80 (dd, $^3J_{H,H}$ = 8.4, $^4J_{H,P}$ = 2.1 Hz, 2 H, H$_f$), 7.84 (s, 1 H, H$_e$) ppm. ^{13}C{^{1}H} NMR ($CDCl_3$): δ = 56.0, 100.6, 113.3 (d, $J_{C,P}$ = 11.9 Hz), 123.1 (d, $J_{C,P}$ = 1.2 Hz), 124.8, 128.2, 128.7 (d, $J_{C,P}$ = 62.6 Hz), 129.0, 129.3 (d, $J_{C,P}$ = 15.5 Hz), 129.4 (d, $J_{C,P}$ = 12.1 Hz), 132.2 (d, $J_{C,P}$ = 2.6 Hz), 134.3 (d, $J_{C,P}$ = 14.0 Hz), 138.9 (d, $J_{C,P}$ = 2.6 Hz), 141.4, 155.8, 160.6, 163.4 ppm. ^{31}P{^{1}H} NMR ($CDCl_3$): δ = 32.7 ppm. UV/Vis (CH_2Cl_2): λ_{max} (ε) = 350 (25700 M^{-1} cm^{-1}). IR: $\tilde{\nu}$ = 326.83 (ν_{Au-Cl}), 1653 ($\nu_{C=O}$) cm^{-1}. HRMS (ESI): calcd. for $C_{28}H_{21}AuClO_3PNa$ 691.04746 [M + Na]$^+$; found 691.04815.

[(3-{4-(Diphenylphosphanyl)phenyl}-7-methoxy-2*H*-chromen-2-one)gold(I)(thio-β-D-glucose tetraacetate)] (CP-AuS-2): The reaction was carried out under argon. [(3-{4-(Diphenylphosphanyl)phenyl}-7-methoxy-2*H*-chromen-2-one)AuCl] (CP-Au-2; 128mg, 0.193 mmol) was dissolved in degassed CH_2Cl_2 (10 mL). 1-Thio-β-D-glucose tetraacetate (70.3 mg, 0.193 mmol) dissolved in distilled acetone (5 mL), NaOH (7.7 mg, 0.193 mmol) and four drops of water were introduced into a Schlenk tube. The reaction mixture was stirred for 10 min at room temperature in the dark. This mixture was slowly added to the first one at 0 °C and then stirred for 3 h at room temperature in the dark. The reaction mixture was filtered to remove salts and the solvent was removed under reduced pressure. The complex CP-AuS-2 was isolated as a yellow powder (177 mg, 92 % yield). ^{1}H NMR ($CDCl_3$): δ = 1.90 [s, 3 H, C*H*$_3$C(O)], 1.97 [s, 3 H, C*H*$_3$C(O)], 2.02 [s, 3 H, C*H*$_3$C(O)], 2.05 [s, 3 H, C*H*$_3$C(O)], 3.74–3.80 (m, s, C*H*$_2$ sugar), 3.90 (s, 3 H, H$_a$), 4.13 (dd, $^3J_{H,H}$ = 12.3, $^2J_{H,H}$ = 2.6 Hz, 1 H, C*H*$_2$ sugar), 4.22 (dd, $^3J_{H,H}$ = 12.3, $^3J_{H,H}$ = 4.8 Hz, 1 H, C*H*CH$_2$ sugar), 5.0–5.2 (m, 4 H, C*H* sugar), 6.86 (d, $^4J_{H,H}$ = 2.4 Hz, 1 H, H$_b$), 6.89 (dd, $^3J_{H,H}$ = 8.4, $^4J_{H,H}$ = 2.4 Hz, 1 H, H$_c$), 7.45–7.65 (m, 13 H, H$_{d,g,h,i,j}$), 7.83 (dd, $^3J_{H,H}$ = 8.4, $^4J_{H,P}$ = 2.0 Hz, 2 H, H$_f$), 7.88 (s, 1 H, H$_e$) ppm. ^{13}C{^{1}H} NMR ($CDCl_3$): δ = 20.7, 20.7, 20.7, 21.1, 55.9, 74.2, 74.8, 100.5, 113.1 (d, $J_{C,P}$ = 1.3 Hz), 123.1 (d, $J_{C,P}$ = 1.2 Hz), 128.9, 129.1, 129.3, 129.3 (d, $J_{C,P}$ = 11.4 Hz), 131.9 (d, $J_{C,P}$ = 2.8 Hz), 134.3 (d, $J_{C,P}$ = 13.6 Hz), 138.6, 141.3, 155.6, 160.5, 163.3, 169.6, 170.3, 170.8 ppm. ^{31}P{^{1}H} NMR ($CDCl_3$): δ = 36.2 ppm. UV/Vis (CH_2Cl_2): λ_{max} (ε) = 350 (24300 M^{-1} cm^{-1}). IR: $\tilde{\nu}$ = 370.55 ($\nu_{Au-Sucre}$), 1653 ($\nu_{C=O}$) cm^{-1}. HRMS (ESI): calcd. for $C_{42}H_{40}O_{12}SPAuNa^+$ 1019.15413 [M + Na]$^+$; found 1019.15672.

[(η^6-*p*-Cymene)(3-{4-(diphenylphosphanyl)phenyl}-7-methoxy-2*H*-chromen-2-one)RuCl$_2$] (CP-Ru-2): The reaction was carried out under argon. 3-[4-(Diphenylphosphino)phenyl]-7-methoxy-2*H*-chromen-2-one (CP-2; 150 mg, 0.344 mmol) and [$RuCl_2$(*p*-cymene)]$_2$ (105 mg, 0.172 mmol) were dissolved in degassed CH_2Cl_2 (10 mL). The resulting mixture was stirred at room temperature for 2 h. The reaction was monitored by ^{31}P NMR spectroscopy. Upon completion, the solvent was removed under reduced pressure. The ruthenium complex CP-Ru-2 was isolated as a red powder (222 mg, 87 %

yield). ^{1}H NMR ($CDCl_3$): δ = 1.10 [d, $^3J_{H,H}$ = 7.0 Hz, 6 H, CH(CH_3)$_2$ *p*-cymene], 1.88 (s, 3 H, CH_3 *p*-cymene), 2.84 [hept, $^3J_{H,H}$ = 7.0 Hz, 1 H, $CH(CH_3)_2$ *p*-cymene], 3.87 (s, 3 H, H_a), 5.02 (d, $^3J_{H,H}$ = 6.2 Hz, 2 H, CH_{Ar} *p*-cymene), 5.21 (d, $^3J_{H,H}$ = 6.2 Hz, 2 H, CH_{Ar} *p*-cymene), 6.80–6.89 (m, 2 H, $H_{b,c}$), 7.33–7.45 (m, 7 H, $H_{d,g}$, H_{Ph}), 7.67 (dd, $^3J_{H,H}$ = 8.4, $^4J_{H,P}$ = 2.1 Hz, 2 H, H_f), 7.75 (s, 1 H, H_e), 7.81–7.94 (m, 6 H, H_{Ph}) ppm. ^{13}C{^{1}H} NMR ($CDCl_3$): δ = 17.9, 22.0, 30.4, 55.8, 87.3 (d, $J_{C,P}$ = 5.4 Hz), 89.1 (d, $J_{C,P}$ = 3.3 Hz), 96.2, 100.6, 111.2 (d, $J_{C,P}$ = 3.3 Hz), 113.0, 113.3, 123.8 (d, $J_{C,P}$ = 1.0 Hz), 127.8 (d, $J_{C,P}$ = 10.4 Hz), 128.2 (d, $J_{C,P}$ = 9.9 Hz), 129.3, 130.4 (d, $J_{C,P}$ = 2.1 Hz), 133.7 (d, $J_{C,P}$ = 45.7 Hz), 134.0 (d, $J_{C,P}$ = 45.7 Hz), 134.5 (d, $J_{C,P}$ = 9.4 Hz), 134.7 (d, $J_{C,P}$ = 9.4 Hz), 136.9 (d, $J_{C,P}$ = 2.8 Hz), 141.0, 155.6, 160.8, 163.1 ppm. ^{31}P{^{1}H} NMR ($CDCl_3$): δ = 23.9 ppm. UV/Vis (CH_2Cl_2): λ_{max} (ε) = 348 (31000 M^{-1} cm^{-1}). IR: $\tilde{\nu}$ = 1653 ($\nu_{C=O}$) cm^{-1}. HRMS (ESI): calcd. for $C_{38}H_{35}Cl_2O_3PRu$ 707.10577 [M – Cl]$^+$; found 707.10608; calcd. for $C_{38}H_{35}Cl_2O_3PRuNa$ 765.06412 [M + Na]$^+$; found 765.06388.

[(η^6-*p*-Cymene)(3-{4-(diphenylphosphanyl)phenyl}-7-methoxy-2*H*-chromen-2-one)OsCl$_2$] (CP-Os-2): The reaction was carried out under argon. CP-2 (150 mg, 0.344 mmol) and [$OsCl_2$(*p*-cymene)]$_2$ (136 mg, 0.172 mmol) were dissolved in degassed CH_2Cl_2 (12 mL). The resulting mixture was stirred at room temperature for 2 h. The reaction was monitored by ^{31}P NMR spectroscopy. Upon completion, the solvent was removed under reduced pressure. The osmium complex CP-Os-2 was isolated as a pale-brown powder (215 mg, 75 % yield). ^{1}H NMR ($CDCl_3$): δ = 1.16 [d, $^3J_{H,H}$ = 6.9 Hz, 6 H, CH(CH_3)$_2$ *p*-cymene], 1.99 (s, 3 H, CH_3 *p*-cymene), 2.74 [hept, $^3J_{H,H}$ = 6.9 Hz, 1 H, $CH(CH_3)_2$ *p*-cymene], 3.88 (s, 3 H, H_a), 5.20 (d, $^3J_{H,H}$ = 5.9 Hz, 2 H, CH_{Ar} *p*-cymene), 5.41 (d, $^3J_{H,H}$ = 5.9 Hz, 2 H, CH_{Ar} *p*-cymene), 6.83–6.89 (m, 2 H, $H_{b,c}$), 7.33–7.41 (m, 6 H, H_g, H_{Ph}), 7.43 (d, $^3J_{H,H}$ = 8.4 Hz, 1 H, H_d), 7.68 (dd, $^3J_{H,H}$ = 8.4, $^4J_{H,P}$ = 2.1 Hz, 2 H, H_f), 7.75–7.88 (m, 7 H, H_e, H_{Ph}) ppm. ^{13}C{^{1}H} NMR ($CDCl_3$): δ = 18.0, 22.3, 30.2, 56.0, 80.1 (d, $J_{C,P}$ = 5.0 Hz), 80.6 (d, $J_{C,P}$ = 2.8 Hz), 88.8, 100.6, 103.5 (d, $J_{C,P}$ = 3.9 Hz), 113.1, 113.4, 123.8 (d, $J_{C,P}$ = 1.1 Hz), 127.8 (d, $J_{C,P}$ = 10.4 Hz), 128.1 (d, $J_{C,P}$ = 10.2 Hz), 129.3, 130.5 (d, $J_{C,P}$ = 2.2 Hz), 133.2 (d, $J_{C,P}$ = 52.3 Hz), 133.6 (d, $J_{C,P}$ = 52.3 Hz), 134.6 (d, $J_{C,P}$ = 9.4 Hz), 134.9 (d, $J_{C,P}$ = 9.4 Hz), 136.8 (d, $J_{C,P}$ = 2.4 Hz), 141.0, 155.6, 160.8, 163.1 ppm. ^{31}P{^{1}H} NMR ($CDCl_3$): δ = –13.3 ppm. UV/Vis (CH_2Cl_2): λ_{max} (ε) = 350 (28800 M^{-1} cm^{-1}). IR: $\tilde{\nu}$ = 1653 ($\nu_{C=O}$) cm^{-1}. HRMS (ESI): calcd. for $C_{38}H_{35}Cl_2O_3POs$ – Cl 797.1628 [M – Cl]$^+$; found 797.16421.

[Bis(3-{4-(diphenylphosphanyl)phenyl}-7-methoxy-2*H*-chromen-2-one)PtCl$_2$] (CP-Pt-2): The reaction was carried out under argon. CP-2 (150 mg, 0.344 mmol) and cyclooctadieneplatinum(II) dichloride (64.3 mg, 0.172 mmol) were dissolved in degassed CH_2Cl_2 (10 mL). The resulting mixture was stirred at room temperature for 2 h. The reaction was monitored by ^{31}P NMR spectroscopy. Upon completion, the solvent was removed under reduced pressure. The platinum complex CP-Pt-2 was isolated as a yellow powder (360 mg, 92 % yield). ^{1}H NMR ($CDCl_3$): δ = 3.89 (s, 6 H, H_a), 6.83 (d, $^4J_{H,H}$ = 2.4 Hz, 1 H, H_b), 6.87 (dd, $^3J_{H,H}$ = 8.6, $^4J_{H,H}$ = 2.4 Hz, 1 H, H_c), 7.18–7.26 (m, 8 H, H_i), 7.32–7.80 (m, 22 H, $H_{d,f,g,h,j}$), 7.83 (br. s, 2 H, H_e) ppm. ^{13}C{^{1}H} NMR ($CDCl_3$): δ = 56.0, 100.5, 113.2 (d, $J_{C,P}$ = 12.4 Hz), 123.2, 127.8 (pseudo t, J = 5.6 Hz), 128.2 (pseudo t, J = 5.6 Hz), 129.6, 131.2, 134.5 (pseudo t, J = 5.4 Hz), 135.2 (pseudo t, J = 5.2 Hz), 137.4, 141.4, 155.6, 160.7, 163.2 ppm. ^{31}P{^{1}H} NMR ($CDCl_3$): δ = 13.5 (s+d, $^1J_{P,Pt}$ = 3675 Hz) ppm. UV/Vis (CH_2Cl_2): λ_{max} (ε) = 350 (58300 M^{-1} cm^{-1}). IR: $\tilde{\nu}$ = 1653 ($\nu_{C=O}$) cm^{-1}. HRMS (ESI): calcd. for $C_{56}H_{42}ClO_6P_2Pt$ 1102.17921 [M – Cl]$^+$; found 1102.17991.

Photophysical Characterization: UV/Vis absorption spectra were recorded with a JASCO V630BIO spectrometer. The steady-state fluorescence emission spectra were recorded with a JASCO FP8560 spectrofluorimeter. All fluorescence spectra were corrected for instrument response. The fluorescence quantum yields (Φ_F) were calculated from Equation (1)

$$\frac{\Phi_F}{\Phi_{FR}} = \frac{n^2}{n_R^2} \times \frac{\int_0^\infty I_F(\lambda_E,\lambda_F)d\lambda_F}{\int_0^\infty I_{FR}(\lambda_E,\lambda_F)d\lambda_F} \times \frac{1-10^{-A_R(\lambda_E)}}{1-10^{-A(\lambda_E)}} \quad (1)$$

in which Φ_F and Φ_{FR} are the fluorescence quantum yields of the compound and the reference, respectively, $A(\lambda_E)$ and $A_R(\lambda_E)$ are the absorbances at the excitation wavelength of the compound and the reference, respectively, and n is the refractive index of the medium, and I_F and I_{FR} are the fluorescent intensities of the compound and the reference, respectively. 9,10-Diphenylanthracene (Φ_F = 0.97 in cyclohexane) was used as standard.[10] In all the Φ_F determinations, correction for the solvent refractive index (η) was applied.

X-ray Structures: Suitable crystals of CP-2 and CP-Ru-2 were selected and mounted on a Bruker APEX-II CCD diffractometer. The crystals were kept at 115 K during data collection. Using Olex2,[16] the structures were solved by direct methods using the SHELXT[17] structure solution program and refined by least squares minimization using the SHELXL[18] refinement package. Except for the minor component of a disordered isopropyl group in CP-Ru-2 (C47a and C48a), all non-hydrogen atoms were refined by using anisotropic thermal parameters. Hydrogen atoms were refined by using a riding model.

CCDC 1420552 (for CP-2) and 1420553 (for CP-Ru-2) contain the supplementary crystallographic data for this paper. These data can be obtained free of charge from The Cambridge Crystallographic Data Centre.

Computational Details: The geometries of the singlet ground state (S_0) and the emissive state ($S_{\pi\pi^*}$) were optimized at the B3LYP[19] and TD-B3LYP levels of theory, respectively, for CP-1, CPMe+1, CP-Au-1 and CP-Ru-1. For these optimizations the 6-31G(d) atomic basis set was selected. Relativistic effects were included for the Ru and Pt atoms by using the ECP-28-mwb and ECP-60-mwb Stuttgart/Dresden pseudopotentials.[20] The nature of the stationary points was confirmed by computing the Hessian at the same level of theory. The UV/Vis absorption spectrum was obtained by calculating vertical singlet electronic excitations using TD-B3LYP at the S_0 geometries. Some of the TD-B3LYP calculations were performed in CH_2Cl_2 solution using the polarization continuum model (PCM).[21] The emission excitation energies were obtained by computing the TD-B3LYP excitations for the optimized $S_{\pi\pi^*}$ geometries. All the TD-B3LYP calculations were performed with the same basis set as in the optimizations. All calculations were performed by using the Gaussian09 program package.[22]

Acknowledgments

The authors are grateful to the Centre National de la Recherche Scientifique (CNRS) (ICMUB, UMR CNRS 6302) for financial support. Support was also provided by the Université de Bourgogne and the Conseil Régional de Bourgogne through the 3MIM integrated project (Marquage de Molécules par les Métaux pour l'Imagerie Médicale) and PARI SSTIC n°1 and n°6. Dr. Fanny Picquet, Marie José Penouilh and Dr. Michel Picquet are acknowledged for technical support. E. B. thanks COST Action TD1004 for financial support. D. E. acknowledges the European Research

Council (ERC) (Marches-278845) and the Région des Pays de la Loire for his postdoctoral grant. D. J. acknowledges the European Research Council (ERC) and the Région des Pays de la Loire for financial support within the framework of a starting grant (Marches-278845) and the LUMOMAT project, respectively. This research used the resources of the GENCI-CINES/IDRIS, the Centre de Calcul Intensif des Pays de Loire (CCIPL) and a local Troy cluster.

Keywords: Bioinorganic chemistry · Theranostic agents · Antitumor agents · P ligands · Fluorescent probes

[1] a) A. V. Klein, T. W. Hambley, *Platinum-Based Anticancer Agents*, in: *Ligand Design in Medicinal Inorganic Chemistry* (Ed.: T. Storr), Wiley, Chichester, UK, **2014**, p. 9–10; b) T. C. Johnstone, K. Suntharalingam, S. J. Lippard, *Phil. Trans. R. Soc. A* **2015**, 373:20140185.

[2] a) N. Muhammad, Z. Guo, *Curr. Opin. Chem. Biol.* **2014**, *19*, 144–153; b) C. G. Hartinger, P. J. Dyson, *Chem. Soc. Rev.* **2009**, *38*, 391–401; c) S. Komeda, A. Casini, *Curr. Top. Med. Chem.* **2012**, *12*, 219–235; d) A. F. A. Peacock, P. J. Sadler, *Chem. Asian J.* **2008**, *3*, 1890–1899; e) G. Gasser, I. Ott, N. Metzler-Nolte, *J. Med. Chem.* **2011**, *54*, 3–25; f) E. R. Tiekink, *Inflammopharmacology* **2008**, *16*, 138–142; g) S. Nobili, E. Mini, I. Landini, C. Gabbiani, A. Casini, L. Messori, *Med. Res. Rev.* **2010**, *30*, 550–580; h) I. Ott, *Coord. Chem. Rev.* **2009**, *253*, 1670–1681; i) B. Bertrand, A. Casini, *Dalton Trans.* **2014**, *43*, 4209–4219; j) W. Fiskus, N. Saba, M. Shen, M. Ghias, J. Liu, S. Das Gupta, L. Chauhan, R. Rao, S. Gunewardena, K. Schorno, C. P. Austin, K. Maddocks, J. Byrd, A. Melnick, P. Huang, A. Wiestner, K. N. Bhalla, *Cancer Res.* **2014**, *74*, 2520–2532; k) for examples of clinical trials in progress in 2014–2015, see: https://clinicaltrials.gov/ct2/show/NCT01747798, https://clinicaltrials.gov/ct2/show/NCT01419691 and http://www.cancer.gov/clinicaltrials/search/view?cdrid=743608&version=HealthProfessional#StudyIdInfo_CD0000743608.

[3] R. Kumar, W. S. Shin, K. Sunwoo, W. Y. Kim, S. Koo, S. Bhuniya, J. S. Kim, *Chem. Soc. Rev.* **2015**, DOI: 10.1039/C5CS00224A.

[4] S. S. Kelkar, T. M. Reineke, *Bioconjugate Chem.* **2011**, *22*, 1879–1903.

[5] M. Ali, L. Dondaine, A. Adolle, C. Sampaio, F. Chotard, P. Richard, F. Denat, A. Bettaieb, P. Le Gendre, V. Laurens, C. Goze, C. Paul, E. Bodio, *J. Med. Chem.* **2015**, *58*, 4521–4528.

[6] J. J. Hanthorn, E. Haidasz, P. Gebhardt, D. A. Pratt, *Chem. Commun.* **2012**, *48*, 10141–10143.

[7] S. Tasan, O. Zava, B. Bertrand, C. Bernhard, C. Goze, M. Picquet, P. Le Gendre, P. Harvey, F. Denat, A. Casini, E. Bodio, *Dalton Trans.* **2013**, *42*, 6102–6109.

[8] The value of the coupling constant $^1J_{P\text{-}Pt}$ depends on the nature of the other ligands coordinated to the Pt center and notably on the nature of the ligand *trans* to the P atom. $^1J_{P\text{-}Pt}$ > 3000 Hz values are generally observed for *trans*-[P–PtXY–Cl] complexes, whereas lower coupling constants ($^1J_{P\text{-}Pt}$ < 3000 Hz) are reported for *trans*-[P–PtXY–P] and *trans*-[P–PtXY–olefin] complexes, see, for example: a) L. Rigamonti, A. Forni, M. Manassero, C. Manassero, A. Pasini, *Inorg. Chem.* **2010**, *49*, 123–135; b) A. Massard, V. Rampazzi, A. Perrier, E. Bodio, M. Picquet, P. Richard, J.-C. Hierso, P. Le Gendre, *Organometallics* **2012**, *31*, 947–958; c) J. A. Feducia, M. R. Gagne, *J. Am. Chem. Soc.* **2008**, *130*, 592–599.

[9] Crystal data for CP-2: $C_{28}H_{21}O_3P$ (M = 436.42 g/mol), triclinic, space group $P\bar{1}$ (no. 2), a = 6.5730(4), b = 10.3480(6), c = 16.5877(10) Å, α = 84.354(2), β = 81.001(2), γ = 87.0180(10)°, V = 1108.19(11) Å^3, Z = 2, T = 115 K, μ(Mo-K_α) = 0.152 mm^{-1}, $D_{calcd.}$ = 1.308 g/cm^3, 34563 reflections measured (4.994° ≤ 2θ ≤ 55.23°), 5143 unique (R_{int} = 0.0223, R_{sigma} = 0.0126), which were used in all calculations. The final R_1 value was 0.0322 [$I > 2\sigma(I)$] and wR_2 was 0.0879 (all data). Crystal data for CP-Ru-2: $C_{77}H_{71}Cl_6O_6P_2Ru_2$ (M = 1569.11 g/mol), monoclinic, space group $P2_1/n$ (no. 14), a = 12.3001(6), b = 25.1497(12), c = 22.1034(12) Å, β = 99.4300(10)°, V = 6745.2(6) Å^3, Z = 4, T = 115 K, μ(Mo-K_α) = 0.788 mm^{-1}, $D_{calcd.}$ = 1.545 g/cm^3, 88328 reflections measured (3.726° ≤ 2θ ≤ 55.168°), 15493 unique (R_{int} = 0.0527, R_{sigma} = 0.0415), which were used in all calculations. The final R_1 value was 0.0377 [$I > 2\sigma(I)$] and $wR_2$was 0.0889 (all data). CCDC 1420552 (for CP-2) and 1420553 (for CP-Ru-2) contain the supplementary crystallographic data for this paper. These data are provided free of charge by The Cambridge Crystallographic Data Centre.

[10] A. M. Brouwer, *Pure Appl. Chem.* **2011**, *83*, 2213–2228.

[11] M. Savarese, U. Raucci, C. Adamo, P. A. Netti, I. Ciofinic, N. Rega, *Phys. Chem. Chem. Phys.* **2014**, *16*, 20681–20688.

[12] a) D. Escudero, E. Heuser, R. J. Meier, M. Schäferling, W. Thiel, E. Holder, *Chem. Eur. J.* **2013**, *19*, 15639–15644; b) J.-L. Heully, F. Alary, M. Boggio-Pasqua, *J. Chem. Phys.* **2009**, *131*, 184308.

[13] A. R. Santos, D. Escudero, L. González, G. Orellana, *Chem. Asian J.* **2015**, *10*, 622–629.

[14] "X-type" ligands are ligands that donate one electron to the metal and accept one from it when using the neutral ligand method of electron counting.

[15] a) S. Tasan, C. Licona, P.-E. Doulain, C. Michelin, C. P. Gros, P. Le Gendre, P. D. Harvey, C. Paul, C. Gaiddon, E. Bodio, *J. Biol. Inorg. Chem.* **2015**, *20*, 143–154; b) P. D. Harvey, S. Tasan, C. P. Gros, C. H. Devillers, P. Richard, P. Le Gendre, E. Bodio, *Organometallics* **2015**, *34*, 1218–1227.

[16] O. V. Dolomanov, L. J. Bourhis, R. J. Gildea, J. A. K. Howard, H. Puschmann, *J. Appl. Crystallogr.* **2009**, *42*, 339–341.

[17] G. M. Sheldrick, *Acta Crystallogr., Sect. A* **2015**, *71*, 3–8.

[18] G. M. Sheldrick, *Acta Crystallogr., Sect. A* **2008**, *64*, 112–122.

[19] a) A. D. Becke, *J. Chem. Phys.* **1993**, *98*, 5648–5652; b) C. T. Lee, W. T. Yang, R. G. Parr, *Phys. Rev. B* **1988**, *37*, 785–789.

[20] D. Andrae, U. Häusermann, M. Dolg, H. Stoll, H. Preuss, *Theor. Chim. Acta* **1990**, *77*, 123–141.

[21] a) M. Cossi, V. Barone, B. Menucci, J. Tomasi, *Chem. Phys. Lett.* **1998**, *286*, 253–260; b) B. Menucci, J. Tomasi, *J. Chem. Phys.* **1997**, *106*, 5151–5158.

[22] M. J. Frisch, G. W. Trucks, H. B. Schlegel, G. E. Scuseria, M. A. Robb, J. R. Cheeseman, G. Scalmani, V. Barone, B. Mennucci, G. A. Petersson, H. Nakatsuji, M. Caricato, X. Li, H. P. Hratchian, A. F. Izmaylov, J. Bloino, G. Zheng, J. L. Sonnenberg, M. Hada, M. Ehara, K. Toyota, R. Fukuda, J. Hasegawa, M. Ishida, T. Nakajima, Y. Honda, O. Kitao, H. Nakai, T. Vreven, J. A. Montgomery Jr., J. E. Peralta, F. Ogliaro, M. Bearpark, J. J. Heyd, E. Brothers, K. N. Kudin, V. N. Staroverov, R. Kobayashi, J. Normand, K. Raghavachari, A. Rendell, J. C. Burant, S. S. Iyengar, J. Tomasi, M. Cossi, N. Rega, J. M. Millam, M. Klene, J. E. Knox, J. B. Cross, V. Bakken, C. Adamo, J. Jaramillo, R. Gomperts, R. E. Stratmann, O. Yazyev, A. J. Austin, R. Cammi, C. Pomelli, J. W. Ochterski, R. L. Martin, K. Morokuma, V. G. Zakrzewski, G. A. Voth, P. Salvador, J. J. Dannenberg, S. Dapprich, A. D. Daniels, Ö. Farkas, J. B. Foresman, J. V. Ortiz, J. Cioslowski, D. J. Fox, *Gaussian 09*, revision A.1, Gaussian, Inc., Wallingford, CT, **2009**.

Received: November 9, 2015
Published Online: January 5, 2016